

Structural and Dynamical Trends in Alkali-Metal Silanides Characterized by Neutron-Scattering Methods

Wan Si Tang,^{*,†,‡} Mirjana Dimitrievska,^{*,†,§} Jean-Noël Chotard,^{||} Wei Zhou,[†] Raphaël Janot,^{||} Alexander V. Skripov,[⊥] and Terrence J. Udovic[†]

[†]NIST Center for Neutron Research, National Institute of Standards and Technology, Gaithersburg, Maryland 20899-6102, United States

[‡]Department of Materials Science and Engineering, University of Maryland, College Park, Maryland 20742-2115, United States

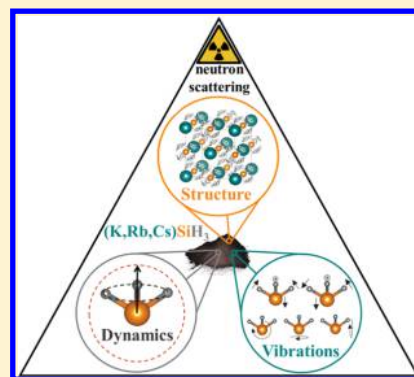
[§]National Renewable Energy Laboratory, Golden, Colorado 80401, United States

^{||}Laboratoire de Réactivité et Chimie des Solides (LRCS), UMR 7314 CNRS, Université de Picardie Jules Verne, 33 rue Saint-Leu, 80039 Amiens Cedex, France

[⊥]Institute of Metal Physics, Ural Branch of the Russian Academy of Sciences, Ekaterinburg 620990, Russia

S Supporting Information

ABSTRACT: Structural, vibrational, and dynamical properties of the mono- and mixed-alkali silanides (MSiH_3 , where $M = \text{K, Rb, Cs, K}_{0.5}\text{Rb}_{0.5}, \text{K}_{0.5}\text{Cs}_{0.5}$, and $\text{Rb}_{0.5}\text{Cs}_{0.5}$) were investigated by various neutron experiments, including neutron powder diffraction (NPD), neutron vibrational spectroscopy (NVS), neutron-scattering fixed-window scans (FWSs), and quasielastic neutron scattering (QENS) measurements. Structural characterization showed that the mixed compounds exhibit disordered (α) and ordered (β) phases for temperatures above and below about 200–250 K, respectively, in agreement with their monoalkali correspondents. Vibrational and dynamical properties are strongly influenced by the cation environment; in particular, there is a red shift in the band energies of the librational and bending modes with increasing lattice size as a result of changes in the bond lengths and force constants. Additionally, slightly broader spectral features are observed in the case of the mixed compounds, indicating the presence of structural disorder caused by the random distribution of the alkali-metal cations within the lattice. FWS measurements upon heating showed that there is a large increase in reorientational mobility as the systems go through the order–disorder (β – α) phase transition, and measurements upon cooling of the α -phase revealed the known strong hysteresis for reversion back to the β -phase. Interestingly, at a given temperature, among the different alkali silanide compounds, the relative reorientational mobilities of the SiH_3^- anions in the α - and β -phases tended to decrease and increase, respectively, with increasing alkali-metal mass. This dynamical result might provide some insights concerning the enthalpy–entropy compensation effect previously observed for these potentially promising hydrogen storage materials.



1. INTRODUCTION

Recent theoretical and experimental investigations of the alkali silanide (MSiH_3 , $M = \text{K, Rb, and Cs}$) compounds^{1–3} have fostered further interest within the hydrogen storage community.^{4,5} This new family of complex hydrides was found to store hydrogen reversibly through a MSi/MSiH_3 equilibrium, with a hydrogen equilibrium pressure of ca. 0.1 MPa at 410 K for all three systems. This is largely due to the enthalpy–entropy compensation effect, where a larger cation induces simultaneous linear increases in the changes in enthalpy (ΔH_{des}) and entropy (ΔS_{des}) of the systems, correlating a more stable silanide with more localized H atoms.³ The systems are completely reversible³ and have good cycling retention properties.¹ This reversibility occurs even with huge volume changes (>50%) between the Zintl and hydride phases, the largest ever observed during hydrogen absorption–desorption cycling.^{1,3}

The structure of α - MSiH_3 ($M = \text{K, Rb, and Cs}$) was first solved by powder X-ray diffraction (PXRD)^{6–8} more than half a century ago. All three isostructural phases crystallize in the cubic $\text{NaCl } Fm\bar{3}m$ space group, but the hydrogen positions remained unknown. Subsequently, a different low-temperature β -phase of KSiH_3 was observed upon cooling (273–278 K).⁹ From PXRD, the β - KSiH_3 phase was found to exhibit orthorhombic $Pnma$ symmetry. The heavier atoms were refined, but the hydrogen positions were solved by Fourier difference mapping, giving short Si–H distances ($d_{\text{Si-H}}$) of 1.42 and 1.44 Å. Solid-state proton nuclear magnetic resonance (^1H NMR) spectroscopy performed at 173 K showed that the SiH_3^- groups were fixed in their positions but underwent rapid

Received: June 30, 2016

Revised: August 18, 2016

Published: September 2, 2016

rotations about their 3-fold symmetry axes at higher temperatures of 373 K.⁸

Interest in these alkali silanides was renewed almost two decades later. Starting with a theoretical approach, the MSi/MSiH₃ equilibrium for M = K was calculated to have a good gravimetric hydrogen storage capacity (4.3 wt %) and predicted to be within the range of practical usage conditions (273–373 K, 0.1–1 MPa of H₂).¹⁰ Although MSiH₃ was traditionally synthesized through a classical wet chemistry method,^{6–9,11,12} this prediction meant that MSiH₃ could be prepared by the direct hydrogenation of MSi Zintl phases. Experimental methods showed that this was indeed possible for M = K, Rb, and Cs,^{1–3} and full absorption (to 3 H/formula unit) at 373 K was completed in 20 h. However, this technique was not as successful for M = Li (ref 13) and Na (ref 2) because the formations of their corresponding silanides were not thermodynamically feasible.³

The structural properties of the high- and low-temperature phases of the MSiH₃ compounds (M = K, Rb, and Cs) were also studied in detail using neutron powder diffraction (NPD) with deuterated samples at different temperatures.³ The β -KSiD₃ phase exhibited orthorhombic *Pnma* symmetry,³ as observed previously for β -KSiH₃. The deuterium positions were refined and found to be close to those reported by Fourier difference mapping,⁹ with larger $d_{\text{Si-D}}$ values of 1.537(8) and 1.545(6) Å. The β -RbSiD₃ and β -CsSiD₃ phases, which were previously undetermined, were found to crystallize slightly differently in the monoclinic *P2₁/m* space group, with average $d_{\text{Si-D}}$ values of 1.529 and 1.547 Å, respectively.³ In all three β -phases, the SiD₃[−] groups were encapsulated in the same 7-coordination arrangement of cations, giving a monocapped trigonal prism.^{3,5} However, a larger cation decreases the symmetry of the polyhedron, which, in turn, influences the interconnectivity. Hence, to accommodate the distortion by larger Rb⁺ and Cs⁺ cations, the unit cell shifts from orthorhombic to monoclinic. There is no apparent disorder in the β -phases, consisting of isolated M⁺ cations and pyramidal silanide SiD₃[−] anions, as described previously.^{8,9}

The α -MSiD₃ phases were confirmed to exhibit cubic *Fm $\bar{3}$ m* symmetry, isostructural with their hydrogenous analogues.^{6–8} The deuterium positions in MSiD₃ (M = K, Rb, and Cs) were resolved and modeled to be in the 96*k* Wyckoff site with an approximate occupancy of 12%, giving an average short $d_{\text{Si-D}}$ value of 1.48 Å.^{1,3} The pair distribution function (PDF) extracted from neutron total scattering data showed longer $d_{\text{Si-D}}$ values of 1.52 Å for KSiD₃ and RbSiD₃.⁵ Large thermal factors obtained from Rietveld refinements reflected significant movements within the unit cell.^{1,3} However, the nature of the orientational disorder, static or dynamic, was still not yet fully understood. Subsequent strong evidence from spectroscopic analysis suggested that the disorder was dynamic.⁵ A very recent quasielastic neutron scattering (QENS) study of α -KSiH₃ and α -RbSiH₃ confirmed this fact.¹⁴ The QENS results showed that the order–disorder (β – α) phase transition leads to dynamical changes associated with rapid reorientational motions of the pyramidal SiH₃[−] ions. The pronounced SiH₃[−] dynamics is the reason for the high entropy observed in the disordered phase. This leads to the low entropy variation for hydrogen absorption/desorption, which is the main reason for the favorable hydrogen storage properties of these materials.

These entropy-driven order–disorder phase transitions are often found to occur in complex hydrides. In many cases, these temperature-induced changes are due to sudden rotations and

reorientations of the anions, leading to increasing multiplicities but partial occupancies of the Wyckoff sites. Literature on the alkali borohydrides (MBH₄, M = Na, K, Rb, and Cs) describing such phenomena dates back to 1953,¹⁵ when Stockmayer and Stephenson concluded that the ordered low-temperature tetragonal structure¹⁶ of NaBH₄ changes to a disordered face-centered cubic structure¹⁷ above 190 K due to increasing rotational freedom of the BH₄[−] anion, as similarly observed in heavier alkali cations.¹⁸ Molar volume changes that usually accompany such transitions are about 5%.⁵

In addition to the pure alkali silanides already known in the literature, mixed-alkali silanides (M_{0.5}M'_{0.5}SiH₃, where M, M' = K, Rb, and Cs), as of yet largely unexplored, are also worthy of study. The MSi alkali silicide Zintl phases (M = Li–Cs) are well-described, with LiSi crystallizing in the *I4₁/a* tetragonal space group,^{13,19,20} NaSi in the *C2/c* monoclinic space group,^{2,21} and MSi for M = K, Rb, and Cs in the *P43n* cubic space group,^{1–3,22} Recently, a mixed-alkali silicide was reported by Waibel et al., showing that the K_{1.95}Rb_{2.05}Si₄ phase crystallized in the same *P43n* cubic space group as the pure ones.²³ Because mixed silicide phases are possible, the corresponding mixed-alkali silanides can be prepared by direct hydrogenation of the starting Zintl phases. Such mixed silanides would enable comparison with the pure silanides and potentially aid in the understanding of the role of the cation in the disorder and entropy of the congeners.

In this article, we report the use of various neutron-scattering techniques to characterize the structures and possible SiH₃[−] reorientational dynamics of both the α - and β -phases of the mixed-alkali silanides (M_{0.5}M'_{0.5}SiH₃, where M, M' = K, Rb, and Cs) and how they relate to the structures and dynamics associated with the pure phases. NPD was used to resolve the various structures of the mixed silanides. Neutron vibrational spectroscopy (NVS) coupled with density functional theory (DFT) computations was used to corroborate these resolved structures. Neutron-scattering fixed-window scans (FWSs) and QENS were used to track the dynamical nature of the SiH₃[−] anions within each phase as a function of temperature. These techniques provide a better understanding of the phase-dependent nature of the possible anion reorientations due to the changes in cationic size in the silanides.

2. EXPERIMENTAL DETAILS

MSi (M = K, Rb, Cs, K_{0.5}Rb_{0.5}, K_{0.5}Cs_{0.5}, and Rb_{0.5}Cs_{0.5}) alloys in amounts on the order of 1 g each were synthesized by high-temperature annealing of 1:1.03 atomic ratios of metal to silicon, using potassium (99.95%, Sigma-Aldrich²⁴), rubidium (99.75%, Alfa Aesar), cesium (99.8%, Alfa Aesar), and silicon (powder, −325 mesh, Sigma-Aldrich) starting materials. All materials were handled in an argon-filled glovebox. Each mixture was arc-weld-sealed within a stainless-steel ampule inside the glovebox. The ampules were typically heated at 1 K min^{−1} from room temperature to 773 K for KSi and to 873 K for all other alloys, where they were held for 48 h before being cooled at 0.2 K min^{−1} back to room temperature. A slight excess of silicon was added to ensure that all of the starting alkali metals were reacted and also to act as a reference standard in NPD experiments. All resulting MSi samples were first activated by evacuation at 473 K for 12 h and then hydrogenated (or deuterated) at 373 K with ca. 5 MPa of hydrogen (or deuterium) for up to 24 h.

All PXRD experiments were performed using the Cu radiation ($\lambda_1 = 1.54056$ Å, $\lambda_2 = 1.54439$ Å) Bruker D8

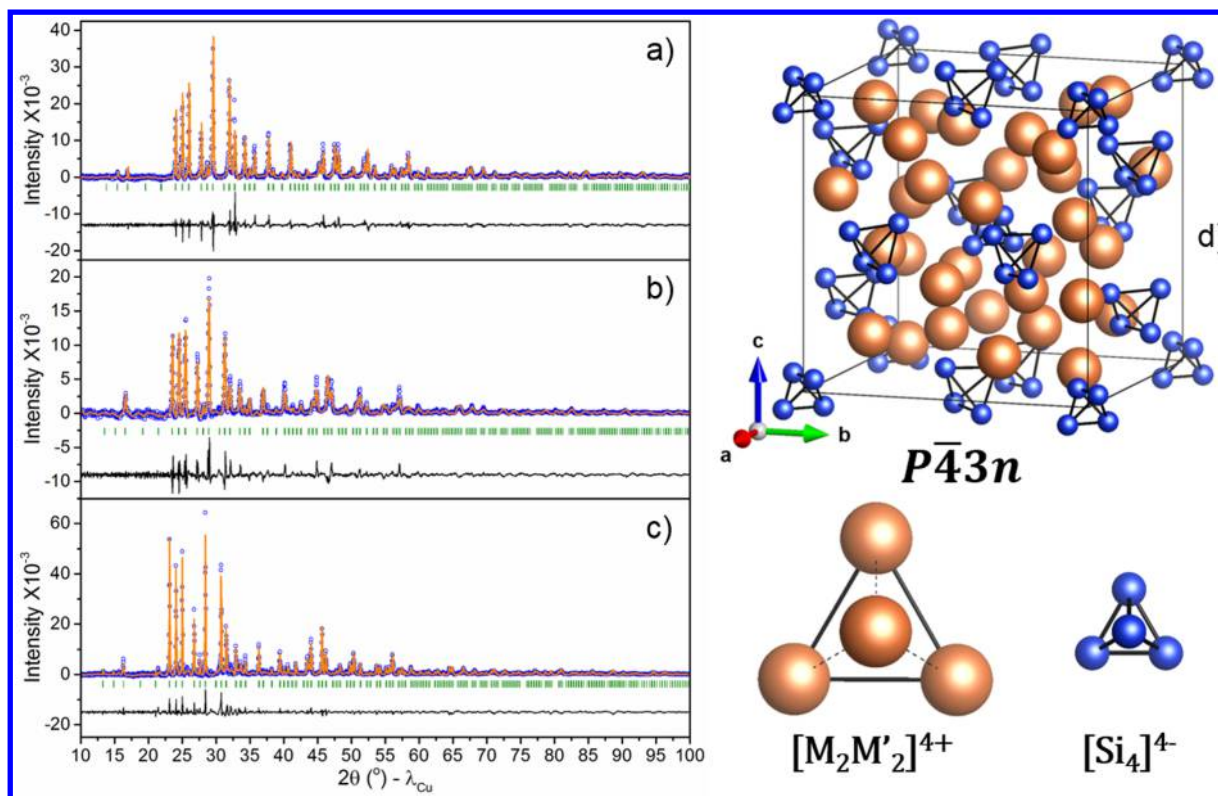


Figure 1. (a–c) Rietveld refinements of the PXRD patterns [experimental (blue circles), fitted (orange line), and difference (black line below observed and calculated patterns) with Bragg peaks (green vertical bars)] for (a) $K_{0.5}Rb_{0.5}Si$, (b) $K_{0.5}Cs_{0.5}Si$, and (c) $Rb_{0.5}Cs_{0.5}Si$ at 293 K (Cu K_{α}). (d) Unit-cell projection of the mixed-alkali silicides in the $P43n$ space group, with enlargements of the tetrahedra formed by the mixed cations $[M_2M'_2]^{4+}$ (orange spheres) and anions $[Si_4]^{4-}$ (blue spheres).

Advance diffractometer equipped with a LynxEye detector, in a room thermostated at 293 K.

To complement the previous structural results for $KSiD_3$, $RbSiD_3$, and $CsSiD_3$, NPD measurements on the deuterated mixed-alkali-metal silanides were performed at the Institut Laue Langevin (ILL, Grenoble, France) on the D1B diffractometer ($\lambda = 1.289 \text{ \AA}$) at 150 and 300 K. Rietveld analysis was performed using the Fullprof software.²⁵ Dicvol²⁶ and Checkcell²⁷ were used in parallel to determine the proper unit cell and possible space groups. All unknown atomic positions were optimized using FOX²⁸ and standardized with STRUCTURE TIDY.²⁹ All structural depictions were generated using VESTA (Visualization for Electronic and Structural Analysis) software.³⁰

All other neutron-scattering measurements were performed on hydrogenated silanides at the National Institute of Standards and Technology (NIST) Center for Neutron Research (NCNR). NVS measurements at 4 K were made on the Filter-Analyzer Neutron Spectrometer (FANS)³¹ using the Cu(220) monochromator with pre- and postcollimations of 20' of arc, yielding a full-width-at-half-maximum (fwhm) energy resolution of about 3% of the neutron energy transfer. Neutron-elastic-scattering FWSs ($\pm 0.5 \text{ K min}^{-1}$) for all compounds were collected between 4 and 340 K on the High-Flux Backscattering Spectrometer (HFBS),³² which operates with 6.27- \AA wavelength neutrons, yielding a resolution of 0.8 μeV fwhm. QENS measurements of $CsSiH_3$ were also made with the Disc Chopper Spectrometer (DCS)³³ between 290 and 350 K utilizing incident neutrons of 2.75 \AA (10.8 meV; medium resolution mode) with a corresponding resolution of 275 μeV fwhm and a maximum momentum transfer (Q) of 4.3 \AA^{-1} . The

instrument resolution function was determined from the measured QENS spectrum at 25 K. All NCNR data were analyzed using the DAVE software package.³⁴

To assist the structural refinements, first-principles calculations were performed within the plane-wave implementation of the generalized gradient approximation to density functional theory (DFT) using a Vanderbilt-type ultrasoft potential with the Perdew–Burke–Ernzerhof exchange correlation.³⁵ A cutoff energy of 544 eV and a $2 \times 2 \times 1$ k -point mesh (generated using the Monkhorst–Pack scheme) were used and found to be sufficient for the total energy to converge within 0.01 meV/atom. For comparison with the NVS measurements, the phonon densities of states (PDOSs) were calculated from the DFT-optimized structure using the supercell method ($2 \times 2 \times 1$ cell size) with finite displacements^{36,37} and were appropriately weighted to take into account the H, Si, K, Rb, and Cs total neutron-scattering cross sections.

For all figures, standard uncertainties are commensurate with the observed scatter in the data, if not explicitly designated by vertical error bars.

3. RESULTS AND DISCUSSION

3.1. Synthesis and Hydrogenation of New Mixed-Alkali-Metal Silicides. With the promising preparation of $K_{1.95}Rb_{2.05}Si_4$ by Waibel et al.,²³ all three mixed-alkali Zintl phases, $K_{0.5}Rb_{0.5}Si$, $K_{0.5}Cs_{0.5}Si$, and $Rb_{0.5}Cs_{0.5}Si$, were likewise synthesized and crystallized in the same $P43n$ cubic space group, with increasing unit-cell parameter values of $a = 12.8315(8)$, $13.0965(7)$, and $13.2982(5) \text{ \AA}$, respectively. Figure 1 shows the corresponding PXRD patterns and the structure of the solid solutions, reminiscent of their individual monoalkali

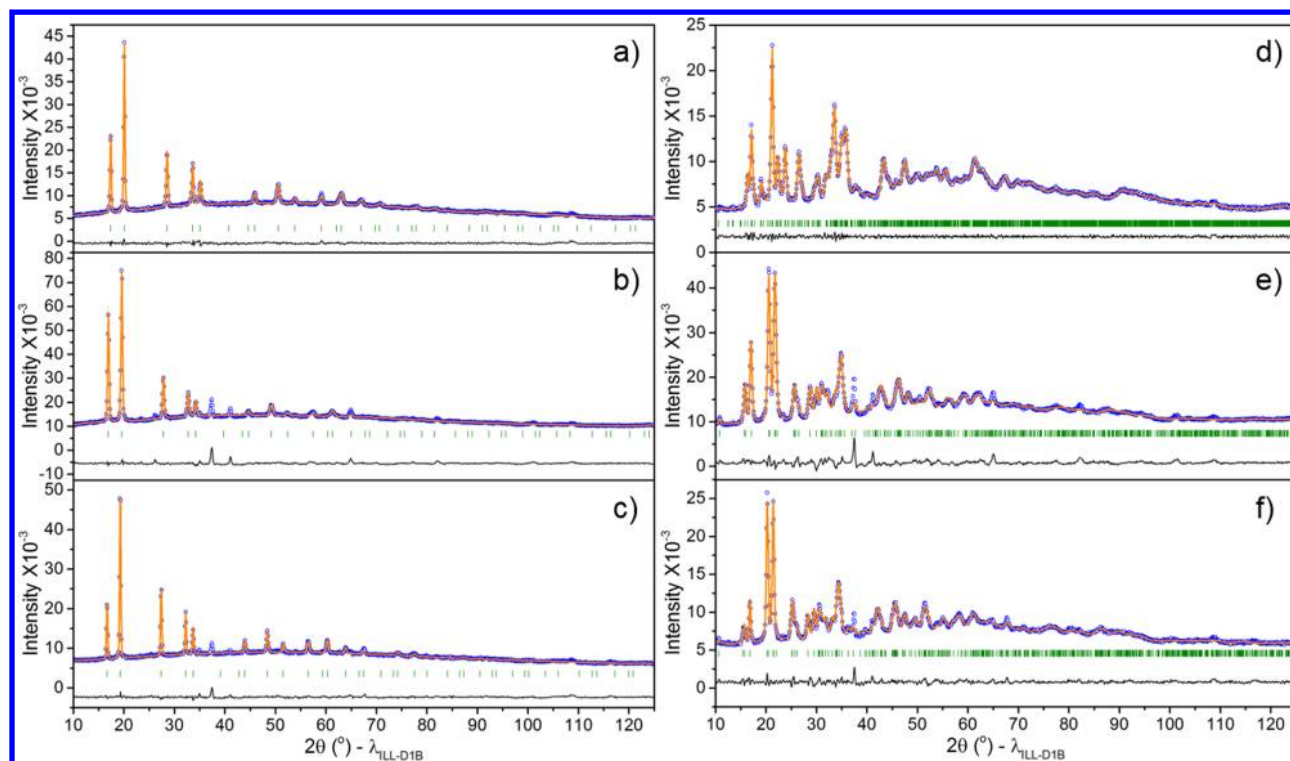


Figure 2. Rietveld refinements of the NPD patterns [experimental (blue circles), fitted (orange line), and difference (black line below observed and calculated patterns) with Bragg peaks (green vertical bars)] for (a) α - $K_{0.5}Rb_{0.5}SiD_3$, (b) α - $K_{0.5}Cs_{0.5}SiD_3$, (c) α - $Rb_{0.5}Cs_{0.5}SiD_3$, (d) β - $K_{0.5}Rb_{0.5}SiD_3$, (e) β - $K_{0.5}Cs_{0.5}SiD_3$, and (f) β - $Rb_{0.5}Cs_{0.5}SiD_3$ compounds. The patterns for the α - and β -phases were collected at 300 and 150 K, respectively, with a wavelength of 1.287 Å. Note: Rietveld refinements were performed on all patterns, with the exception of profile matching for β - $K_{0.5}Rb_{0.5}SiD_3$.

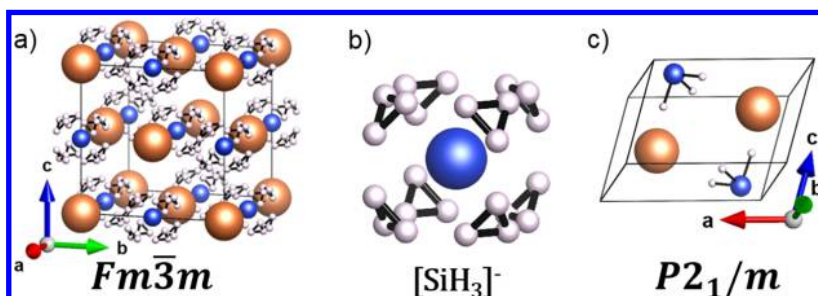


Figure 3. (a) Unit-cell projection for the cubic α - $M_{0.5}M'_{0.5}SiD_3$ (where $M, M' = K, Rb,$ and Cs) phases, in the $Fm\bar{3}m$ space group, with (b) an enlargement of the 96k hydrogen positions around the silicon atom (ca. 12% occupancy). (c) Unit-cell projection of monoclinic β - $K_{0.5}Cs_{0.5}SiD_3$ and β - $Rb_{0.5}Cs_{0.5}SiD_3$ in the $P2_1/m$ space group. Orange, blue, and white spheres denote the M/M' , Si, and H atomic positions, respectively.

phases, but having mixed-alkali cations on the 8e and 24i Wyckoff positions (Table S1). These silicides were found to follow Vegard's law (Figure S1a), as already mentioned by Waibel et al. for the $K_{1.95}Rb_{2.05}Si_4$ phase.²³ Hence, novel mixed-alkali Zintl phases were successfully alloyed.

Subsequently, the hydrogenation of these silicide phases resulted in their corresponding mixed-alkali silanides. Under the reaction conditions as stated for the monoalkali silicides,^{1–3} the $M_{0.5}M'_{0.5}SiH_3$ (or $M_{0.5}M'_{0.5}SiD_3$) ($M, M' = K, Rb,$ and Cs) phases were synthesized with the introduction of 5 MPa of H_2 (or D_2) at 373 K. Structural characterization from PXRD (Figure S2) confirmed that the room-temperature α -phases of the mixtures $K_{0.5}Rb_{0.5}SiD_3$, $K_{0.5}Cs_{0.5}SiD_3$, and $Rb_{0.5}Cs_{0.5}SiD_3$ crystallize in the same $Fm\bar{3}m$ cubic space group as the pure compounds, with increasing unit-cell parameter values of $a = 7.3744(18)$, $7.5784(12)$, and $7.6846(16)$ Å, respectively (Table S2). However, because only the cubic rock-salt (fcc) positions of the mixed-alkali and silicon Wyckoff sites could be positively

identified from PXRD, to better locate the hydrogen positions, deuterated samples of the mixed-alkali phases were further synthesized for NPD.

3.2. Crystal Structures of α - and β -Phases of Mixed-Alkali-Metal Silanides. Figure 2a–c presents the refined NPD patterns measured at 300 K, which correspond to the high-temperature structures for all three mixed-alkali deuterated phases. The results corroborate those from PXRD: The α -phases of the mixtures are isostructural with their hydrogenous analogues in cubic $Fm\bar{3}m$ symmetry^{1–3,6–8} (Figure 3a), with increasing unit-cell parameter values of $a = 7.3826(6)$, $7.5721(18)$, and $7.6888(4)$ Å from refined stoichiometries of $K_{0.50}Rb_{0.5}SiD_{2.88}$, $K_{0.48}Cs_{0.52}SiD_{2.88}$, and $Rb_{0.55}Cs_{0.45}SiD_{2.90}$, respectively (Table S3). The deuterium positions were resolved and modeled to be in the 96k Wyckoff site (Figure 3b) with approximate occupancies of 11.5(1)%, 11.5(3)%, and 11.6(2)%, giving small d_{Si-D} values of 1.479(3), 1.472(8), and 1.480(4) Å, within the SiH_3^- clusters for the respective K–Rb,

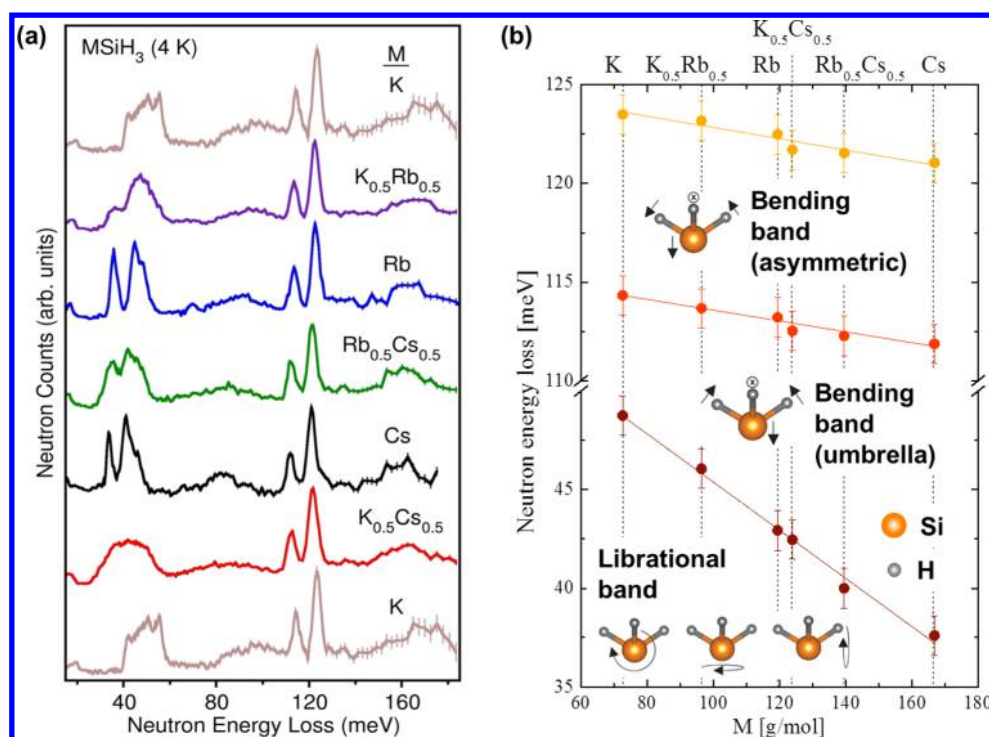


Figure 4. (a) Neutron vibrational spectra at 4 K of the series of β -MSiH₃ compounds ($M = \text{K, Rb, Cs, K}_{0.5}\text{Rb}_{0.5}, \text{K}_{0.5}\text{Cs}_{0.5}, \text{Rb}_{0.5}\text{Cs}_{0.5}$; KSiH₃ spectrum plotted twice to aid comparison). (b) Variation of the average energy of the most intense SiH₃⁻ vibrational bands as a function of the molar mass and illustration of the eigenvectors of the Γ -point vibrational eigenmodes for the corresponding bands obtained from the DFT calculations. Note: The average energies of the modes were determined by fitting the top of the peaks with a Lorentzian function, whereas the error bars correspond to the standard deviation obtained from the fitting.

K–Cs, and Rb–Cs mixed hydrides. Such short silicon–deuterium bond distances have already been observed in the monoalkali silanides.^{1,3} Therefore, the α -phases of the mixed-alkali silanides behave, as expected, similarly to the monoalkali phases. Furthermore, linear relationships between the obtained lattice parameters of the mixtures and the corresponding values for the pure compounds confirm that the α -phase mixtures are indeed alloys (Figure S1b), much like the starting Zintl phases. The refinement gives large B_{iso} values, and the nature of this disorder in the α -phases is addressed in subsequent sections of this work.

To observe the low-temperature β -phases for the mixed-alkali $M_{0.5}M'_{0.5}\text{SiD}_3$ hydrides, NPD patterns were measured for the same samples at 150 K. Indeed, new phases were observed for all three silanides, as shown in Figure 2d–f, and Rietveld refinements were performed to elucidate the structures of these phases (Table S4). The β -K_{0.5}Rb_{0.5}SiD₃ NPD pattern (Figure 2d) resembles much of the orthorhombic $Pnma$ β -KSiD₃ phase,¹ but with some amounts of angular distortion, and was best indexed to a probable monoclinic $P2_1/m$ space group, different from the monoclinic β -phases observed earlier.³ However, solving the structure for this phase was more difficult because of the low resolution of the NPD pattern collected, and further diffraction experiments are in progress. On the other hand, the NPD patterns for β -K_{0.5}Cs_{0.5}SiD₃ and β -Rb_{0.5}Cs_{0.5}SiD₃ (Figure 2e,f) are akin to those of the heavier-alkali silanide phases, and unsurprisingly, both crystallized in a monoclinic structure with the $P2_1/m$ space group (Figure 3c), analogous to β -RbSiD₃ and β -CsSiD₃.³ Average small $d_{\text{Si–D}}$ values of 1.548 Å for β -K_{0.46}Cs_{0.54}SiD_{2.80} [$a = 7.2221(14)$ Å, $b = 5.6019(9)$ Å, $c = 4.9678(8)$ Å, and $\beta = 109.107(13)^\circ$] and 1.582 Å for β -Rb_{0.58}Cs_{0.42}SiD_{2.76} [$a = 7.3054(10)$ Å, $b =$

5.6830(7) Å, $c = 5.0487(7)$ Å, and $\beta = 108.648(10)^\circ$] were found in the SiH₃⁻ units. Similarly to the pure β -phases consisting of discrete anions,^{8,9} the well-defined pyramidal SiD₃⁻ groups with low B_{iso} values are also encapsulated in a 7-coordination arrangement of cations in the mixed-alkali β -phases.^{3,5} A comparison of the β -phases indicates that the interconnectivity of this arrangement is affected by the size of the cations: The unit cell shifts from orthorhombic (K⁺) to monoclinic (Rb⁺, K⁺/Cs⁺, Rb⁺/Cs⁺, Cs⁺) with decreasing symmetry.³ Hence, cationic distortions lead to different crystal chemistries for the β -phases.

The volume-by-multiplicity (V/Z) values for all of the compounds discussed above and the respective changes in volumes for the various transitions are reported in Table S5. Naturally, there is a huge volume change (>50%) when the silicides are hydrogenated into the silanide phases,^{1,3} with an increasing trend when larger cations are incorporated into the rock-salt structure, as seen before.³ However, there is a smaller volume change between the β - and α -polymorphs, with a tighter unit cell for the ordered low-temperature phase, as expected, and the same increasing trend with larger cations. Figure S3 compares the V/Z values of the mono- and mixed-alkali silicides and silanides, and the values follow a linear variation with the average cationic radius of each structure as calculated from refined stoichiometries, reconfirming solid solutions within both congener families. Therefore, the structures of the room-temperature disordered (α) and the low-temperature ordered (β) phases of the mixed-alkali $M_{0.5}M'_{0.5}\text{SiD}_3$ compounds ($M, M' = \text{K, Rb, and Cs}$) resolved by diffraction experiments add to the library of monoalkali analogues for the α - and β -MSiD₃ ($M = \text{K, Rb and Cs}$) phases, previously reported.^{1,3} Evidently, the size of the cations is a

greater factor in the structural symmetry of the ordered β -phases than in that of the disordered α -phases, which largely remains unperturbed in the fcc structure.

3.3. Neutron Vibrational Spectroscopy. Figure 4a compares the neutron vibrational spectra for each of the investigated hydrogenated silanide compounds at 4 K in their ordered β -phases. The total neutron-scattering cross section for H is relatively large compared to those of the alkali-metal elements and Si. Thus, each spectrum reflects a hydrogen-weighted phonon density of states (PDOS) dominated by the optical phonons involving large-amplitude H motions, namely, SiH_3^- librational (torsional) modes yielding a broad structure-dependent band somewhere between 30 and 60 meV and SiH_3^- deformation (bending) modes yielding two narrow bands between 110 and 130 meV ($1 \text{ meV} \approx 8.066 \text{ cm}^{-1}$). The lower-energy deformation band is associated with the SiH_3^- “umbrella” modes (symmetric bending mode). In addition, the more diffuse features evident between 60 and 110 meV and above 130 meV reflect the contributions from two-phonon bands, namely, the combination of the librational or deformation modes with the lower-energy optoacoustic modes involving whole SiH_3^- anion displacements. Similar but slightly broader spectral features are observed in the case of the mixed compounds, indicating an increase in the structural disorder with respect to the pure compounds. This disorder is likely caused by the random distribution of the alkali-metal components in the lattice.

There is a clear trend between the position of the most intense bands in the spectra and the size of the lattice (i.e., molecular weight), with the band positions decreasing with increasing unit-cell volume for both pure compounds and their solid solutions (Figure 4b). For example, CsSiH_3 (with the largest unit-cell volume) yields the lowest average librational band energy, whereas KSiH_3 (with the smallest unit-cell volume) yields the highest. This trend is also true for the positions of the bending mode bands, although the dependency is softer than for the librational mode. Additionally, Figure 4b illustrates the eigenvectors of the zone-center modes corresponding to the presented bands and obtained from DFT calculations. In this case, the described modes involve only SiH_3^- anion vibrations, relative to the fixed metallic cations. The substantially decreased energies of the librational and bending modes in heavier-alkali β - MSiH_3 phases as compared to the lighter-alkali β - MSiH_3 phases are attributed to the M^+ environment ($M = \text{K, Rb, Cs, K}_{0.5}\text{Rb}_{0.5}, \text{K}_{0.5}\text{Cs}_{0.5}, \text{Rb}_{0.5}\text{Cs}_{0.5}$). An increase in the size and mass of the M^+ cations will induce an increase in the bond lengths, which will lead to a reduction in the force constants, concomitantly leading to a decrease in the energy of the vibrational modes. Similar trends in the frequency of the modes were observed in the Raman spectra of KSiH_3 and RbSiH_3 .⁵

Figure 5 compares the neutron vibrational spectra for KSiH_3 , RbSiH_3 , and CsSiH_3 with the simulated PDOSs computed from the experimentally observed structures³ after DFT optimization. Ignoring the expected minor inaccuracies with DFT in predicting absolute band energies, there is good overall qualitative agreement for all three compounds between experiment and theory. In particular, the simulated spectra reproduce the general details of the librational band line shapes (which vary among the three compounds), the two-band structure of the bending modes, and the broad combination bands, as well as the direction of the shifts in band energies with unit-cell volume. More specifics concerning the natures,

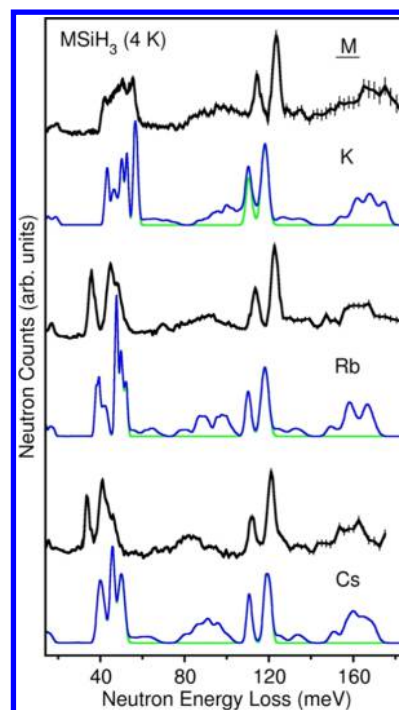


Figure 5. Neutron vibrational spectra (black) of KSiH_3 , RbSiH_3 , and CsSiH_3 at 4 K compared to the simulated one-phonon (green) and one- + two-phonon (blue) densities of states from first-principles phonon calculations of the DFT-optimized low-temperature ordered structures.

symmetries, and energies associated with the individual phonon normal modes for the three compounds can be found in Tables S6–S8 and associated animation files in the Supporting Information.

3.4. Neutron-Scattering Fixed-Window Scans (FWSs).

As a reminder, the FWS measured at zero energy transfer (elastic scattering) is a useful indicator of the temperature-dependent dynamical behavior of H atoms in a material.³⁸ At very low temperature, the H atoms are essentially frozen in place; that is, the motions of H atoms are too slow to be “sensed” within the submicroelectronvolt resolution window of the backscattering spectrometer, and the H atoms appear to scatter neutrons only elastically. As the temperature is first increased above this low point, the FWS intensity drops only slowly due to Debye–Waller attenuation.³⁹ At the same time, at progressively higher temperatures, the frequencies of H motions (localized or diffusive jumps) increase. At about $10^8 \text{ jumps s}^{-1}$, the spectrometer finally begins to sense the H motion as a fraction of the elastic peak begins to broaden, becoming quasielastic. Keeping in mind that the total scattering intensity, elastic and quasielastic, is constant to first order (ignoring the Debye–Waller attenuation), the increasing quasielastic broadening causes the FWS intensity (measured at zero energy transfer) to drop more precipitously. As the H mobility increases above $10^{10} \text{ jumps s}^{-1}$, the quasielastic portion becomes so broad that it disappears into the baseline, and the remaining FWS intensity begins to level off again. Moreover, this second downward-sloping plateau can drop even further than expected from the Debye–Waller attenuation at higher temperatures if the mechanism of the H motion changes to one of increased dimensionality. This is because the fraction of the total scattering intensity that becomes quasielastic is mechanism-dependent.

Figure 6 compares the FWSs for each of the investigated hydrogenated silanide compounds starting at 4 K in the

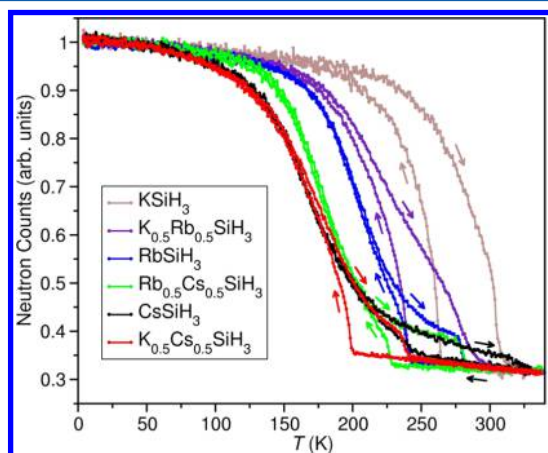


Figure 6. Neutron-elastic-scattering fixed-window scans for the series of MSiH_3 compounds ($M = \text{K}, \text{Rb}, \text{Cs}, \text{K}_{0.5}\text{Rb}_{0.5}, \text{K}_{0.5}\text{Cs}_{0.5}$, and $\text{Rb}_{0.5}\text{Cs}_{0.5}$) summed over detectors covering a Q range from 0.56 to 1.68 \AA^{-1} . Arrows differentiate heating and cooling scans. For a qualitative comparison, the individual data sets were scaled so as to match intensities at both the lowest and highest temperatures for $\text{K}_{0.5}\text{Cs}_{0.5}\text{SiH}_3$.

ordered β -phase, heated across the order–disorder phase transition into the disordered α -phase to a final temperature of 340 K and then cooled back to 4 K. Ideally, it would be preferable to consider only Q values free of coherent Bragg scattering so that the signal predominantly reflects the incoherent scattering from hydrogen. Nonetheless, for markedly better signal-to-noise ratios, detectors were summed together over a Q range of from 0.56 to 1.68 \AA^{-1} . To compensate for the small variations in the measured neutron intensities among samples due to added contributions from coherent Bragg scattering from some of the detectors as well as extra incoherent elastic scattering from possible minor alkali-metal-hydride impurity phases, we scaled and intensity-shifted all of the FWSs so as to match intensities at both the lowest and highest temperatures for $\text{K}_{0.5}\text{Cs}_{0.5}\text{SiH}_3$. In this way, we were able to make a reasonable dynamical comparison among all samples on a similar basis. A comparison of FWSs using individual detectors indicated similar results, justifying the summing of detectors.

The series of FWSs gives a comparative picture of the SiH_3^- dynamical behavior and phase hysteresis for each compound. According to Figure 6, upon heating of the β -phases from 4 K, the two compounds with the most reorientationally mobile SiH_3^- anions at low temperature are CsSiH_3 and $\text{K}_{0.5}\text{Cs}_{0.5}\text{SiH}_3$, which start exhibiting jump frequencies on the order of $10^8 \text{ jumps s}^{-1}$ (as evidenced by the onset of a more pronounced decrease in the FWS intensity with increasing temperature above their initial plateaus) by about 75–80 K. Analogous FWS-intensity behaviors marking similar jump-frequency thresholds are observed at progressively higher temperatures of about 125 K for $\text{Rb}_{0.5}\text{Cs}_{0.5}\text{SiH}_3$, 150 K for RbSiH_3 , 165 K for $\text{K}_{0.5}\text{Rb}_{0.5}\text{SiH}_3$, and 225 K for KSiH_3 . This observed trend in jump-frequency thresholds for the various β -phase compounds indicate decreasing SiH_3^- anion mobilities with decreasing cation size/mass. This might be reasonably expected from a simple steric perspective, because the decrease in unit-cell size with decreasing cation size/mass likely correlates with a

decrease in available interstitial volume for the SiH_3^- anions and thus an increase in their steric barriers to reorientation. This is also a trend that has been observed for BH_4^- anion reorientations in the alkali-metal borohydrides.³⁸

Upon further heating, all compounds except for $\text{K}_{0.5}\text{Rb}_{0.5}\text{SiH}_3$ and KSiH_3 appear to attain, for the most part, their second plateaus (indicative of reaching and even surpassing $10^{10} \text{ jumps s}^{-1}$) before undergoing their full transformation to the disordered α -phases. The steep drops in FWS intensities for $\text{K}_{0.5}\text{Rb}_{0.5}\text{SiH}_3$ and KSiH_3 near 270 and 300 K, respectively, signal that the order–disorder phase changes are occurring before the reorienting SiH_3^- anions have moved above the 10^8 – $10^{10} \text{ jumps s}^{-1}$ frequency window of the spectrometer. For the other compounds, the phase change is marked by a second distinct drop in FWS intensity to a third low-intensity plateau, which strongly suggests that the SiH_3^- anion reorientational mechanism is changing, concomitant with the phase change.

The low FWS intensity for each compound by 340 K (compared to 4 K) clearly signals rapidly reorienting SiH_3^- anions within the disordered cubic α -phase structures. Based on the apparent quasispherical H disorder surrounding each Si atom, as suggested by the current and previous NPD data^{1,3} and indicated by the recent α - KSiH_3 and α - RbSiH_3 QENS study,¹⁴ it is clear that the SiH_3^- anions are undergoing small-jump, H-sphere-tracing reorientations (centered on the Si atoms) at this temperature and unequivocally at jump rates much larger than $10^{10} \text{ jumps s}^{-1}$. This type of three-dimensional motion is consistent with the relatively large drop in FWS intensity observed between 4 and 340 K for all compounds. This is also in agreement with the results from ref 14, where characteristic relaxation times of approximately 0.7 ps were observed for this type of mechanism. The existence of the intermediate-intensity, second plateau for all compounds (except KSiH_3 for reasons mentioned above) just below the order–disorder transition is probably an indication of a more spatially restrictive SiH_3^- anion reorientational mechanism, such as uniaxial 3-fold reorientation about the anion trigonal symmetry axis, which would necessarily result in a smaller fraction of the total scattering intensity becoming quasielastic and a larger fraction remaining elastic. This is expected behavior for systems exhibiting order–disorder transitions. For example, LiBH_4 and the various Li and Na *closo*-boranes routinely display order(s)-of-magnitude jumps in orientational mobility upon transformation to their disordered structures.^{40–42} This behavior can be due to factors such as a volume expansion and/or a change in distortion of the unit cell.

Upon cooling of the α -phase compounds back to 4 K, there is a compound-dependent, hysteretic change back to the ordered β -phases evidenced by a sharp rise in FWS intensities. As the temperature is lowered further and the transformation proceeds to completion for each compound, the FWS intensity from the cooling scan merges and retraces, in reverse, the path taken by the heating scan. The heating and cooling scans for KSiH_3 are particularly noteworthy in that they suggest a somewhat broader temperature range for the transformations between phases. This is consistent with the broader calorimetric peaks for KSiH_3 compared to those for RbSiH_3 and CsSiH_3 , as observed by differential scanning calorimetry.³

3.5. Quasielastic Neutron Scattering (QENS). To complement the results of the previous QENS study of α - KSiH_3 and α - RbSiH_3 ,¹⁴ the SiH_3^- reorientational dynamics for α - CsSiH_3 were further investigated by DCS measurements. A

more complex dynamical behavior reminiscent of a mixed-phase material was observed in the lower-temperature region (<290 K) and will be the subject of a separate article.

QENS spectra for α -CsSiH₃ upon cooling over the temperature range from 350 to 270 K were fitted with a function consisting of one elastic component together with two Lorentzian functions (L_1 and L_2) and a flat background. It should be noted that initial attempts to fit the QENS spectra with only one Lorentzian function did not give satisfying results, which led to the addition of a second very broad Lorentzian (on the order of 10 meV fwhm), which was treated as component containing higher quasielastic structure factors and low-energy inelastic modes, separate from the SiH₃⁻ reorientational hopping motions. A similar fitting procedure was also applied for the analysis of KSiH₃ and RbSiH₃.¹⁴ As an example, Figure 7 presents the fit to the experimental data measured at $T = 310$ K and $Q = 1.2 \text{ \AA}^{-1}$ using 2.75 \AA neutrons.

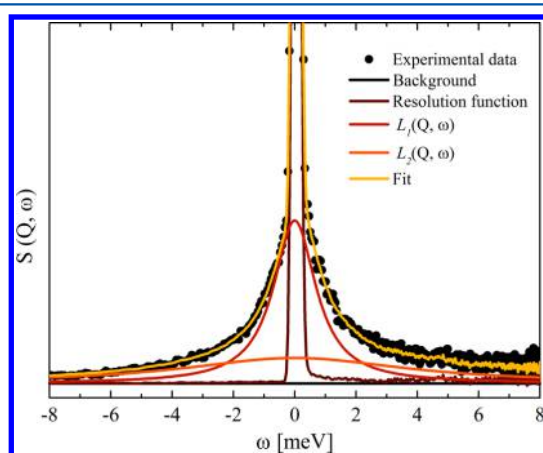


Figure 7. $S(Q, \omega)$ of CsSiH₃ at $T = 310$ K and $Q = 1.2 \text{ \AA}^{-1}$, as measured with 2.75 \AA neutrons with an instrumental resolution line width of $275 \mu\text{eV}$ fwhm.

Figure 8 presents an Arrhenius plot between 270 and 350 K of the quasielastic width of the narrowest component, $\Gamma_1(Q)$ shown in Figure 7, because this represents the fundamental jump correlation frequency. $\Gamma_1(Q)$ follows an Arrhenius dependence with an activation energy of $32(3) \text{ meV}$ for CsSiH₃ over the temperature range reported. (Note that a somewhat higher activation energy was observed upon inclusion of additional QENS widths determined at even lower temperatures down to 190 K, which again will be discussed in a future report.) Figure 8 also shows Arrhenius plots of the quasielastic widths for KSiH₃ and RbSiH₃ with respective activation energies for comparison.¹⁴ We caution that these reorientational barriers reflect some average for each compound over its measured temperature range and might be complicated by the fact that we are dealing with a composite three-dimensional reorientational mechanism comprising both reorientations of H atoms around the 3-fold SiH₃⁻ axis and the 8-fold reorientations of this SiH₃⁻ axis within the disordered α -phase structure.

It is concluded that the activation energies and the reorientational mobility of SiH₃⁻ anions are highly dependent on the cation environment. A decrease in reorientational mobilities is observed with increasing lattice constant (i.e., with increasing size/mass of the cation) in the case of the high-temperature disordered α -phase. Although one might reason-

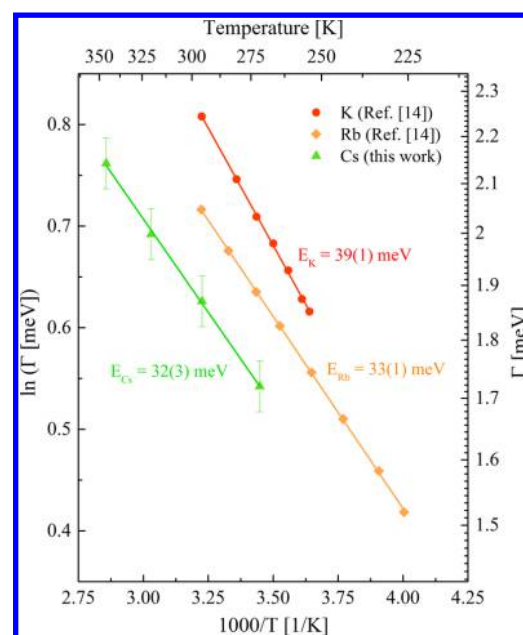


Figure 8. Arrhenius plot of $\Gamma_1(Q)$ for CsSiH₃ measured in this work and comparison with the data for KSiH₃ and RbSiH₃ taken from ref 14. Corresponding activation energies obtained from the fits are labeled next to the data.

ably expect lower reorientational barriers with increasing lattice constant from a steric perspective, the concomitant lower apparent mobilities appear to be rather unusual behavior. We remind the reader that the opposite behavior was detected for the low-temperature ordered β -phase based on the FWS results, where the reorientational mobility of the SiH₃⁻ anions was found to increase with increasing cation size. A better understanding of the trend in relative SiH₃⁻ mobilities for both the β - and α -phase compounds will likely benefit from more rigorous theoretical modeling in conjunction with complementary NMR and more extensive QENS measurements.

It is expected that the variations in the reorientational mobility of SiH₃⁻ anions will affect the thermodynamic properties of the α -phase. If the reorientational mobility of SiH₃⁻ anions is decreasing, then the entropy term corresponding to this state will likely also decrease, making the α -phase effectively less disordered as the cation size increases. This will also lead to an increase in the entropy gain upon dehydrogenation of the α -phase to the metal silicide and gaseous molecular hydrogen with increasing cation size, in agreement with the thermodynamic observations in ref 3.

4. SUMMARY

Various neutron-scattering techniques, including NPD, NVS, FWS, and QENS, and DFT calculations were employed to gain deeper insights into the structural and vibrational properties of the α - and β -phases of both the mono- and mixed-alkali silanides MSiH₃ and $M_{0.5}M'_{0.5}\text{SiH}_3$, where $M, M' = \text{K, Rb, and Cs}$, which have been recently proposed as possible materials for near-ambient hydrogen-storage systems. Structural characterization showed that all mixed-alkali as-synthesized silicides and hydrogenated α -phases crystallized in the $P\bar{4}3n$ and $Fm\bar{3}m$ cubic space groups, respectively, as for their monoalkali counterparts. β -K_{0.5}Cs_{0.5}SiD₃ and β -Rb_{0.5}Cs_{0.5}SiD₃ were found to crystallize in the $P2_1/m$ monoclinic structure, whereas β -

$K_{0.5}Rb_{0.5}SiD_3$ exhibited behavior intermediate between those of its two corresponding pure β -phases. Neutron vibrational spectra of the various β -phase compounds were compared, and the monoalkali versions compared well with the simulated phonon densities of states determined from first-principles calculations. A red shift in the band energies of the librational and bending modes was observed with the increase in the size of the lattice and explained by the influence of the alkali environment on the bond lengths and force constants. Additionally, neutron-scattering FWSs were used to track the dynamical nature of the SiH_3^- anions within each phase as a function of temperature. The results showed distinct drops in the FWS intensity with variations in the temperature that can be explained by the dynamical changes in the SiH_3^- anion reorientational mechanism between the two phases. Moreover, changes in the cation environment and the concomitant changes in unit-cell size were observed to have a direct impact on the reorientational mobility of the SiH_3^- anions and their jump frequencies, with diametrically different trends observed for the α - and β -phases. Although rather unusual behavior from a steric perspective, the observed cation-dependent changes in the reorientational mobility of the α -phase SiH_3^- anions are qualitatively consistent with the increasingly ordered nature of the α -phase with increasing cation size, as previously reported.

■ ASSOCIATED CONTENT

Supporting Information

The Supporting Information is available free of charge on the ACS Publications website at DOI: 10.1021/acs.jpcc.6b06591.

Instructions for generating animations of all vibrational modes contributing to the simulated PDOSs; tables containing structural refinement results, experimental bending-mode energies, and DFT-generated phonon symmetries and energies, and figures showing the refinements (PDF)

CIF file for the NPD-refined structure of α - $K_{0.5}Cs_{0.5}SiH_3$ (CIF)

CIF file for the NPD-refined structure of α - $K_{0.5}Rb_{0.5}SiH_3$ (CIF)

CIF file for the NPD-refined structure of α - $Rb_{0.5}Cs_{0.5}SiH_3$ (CIF)

CIF file for the NPD-refined structure of β - $Rb_{0.5}Cs_{0.5}SiH_3$ (CIF)

CIF file for the NPD-refined structure of β - $K_{0.5}Cs_{0.5}SiH_3$ (CIF)

Data files for generating animations of all vibrational modes contributing to the simulated PDOSs (ZIP)

Data files for generating animations of all vibrational modes contributing to the simulated PDOSs (ZIP)

Data files for generating animations of all vibrational modes contributing to the simulated PDOSs (ZIP)

■ AUTHOR INFORMATION

Corresponding Authors

*E-mail: wansi.tang@nist.gov. Tel.: +1-301-975-8924.

*E-mail: mirjana.dimitrievska@nist.gov, mirjana.dimitrievska@nrel.gov. Tel.: +1-301-975-0403.

Notes

The authors declare no competing financial interest.

■ ACKNOWLEDGMENTS

This work was partially supported by the DOE EERE under Grant No. DE-EE0002978 and utilized facilities supported in part by the National Science Foundation under Agreement DMR-0944772. M. D. gratefully acknowledges research support from the U.S. Department of Energy, Office of Energy Efficiency and Renewable Energy, Fuel Cell Technologies Office, under Contract No. DE-AC36-08GO28308.

■ REFERENCES

- (1) Chotard, J.-N.; Tang, W. S.; Raybaud, P.; Janot, R. Potassium Silanide ($KSiH_3$): A Reversible Hydrogen Storage Material. *Chem. - Eur. J.* **2011**, *17* (44), 12302–12309.
- (2) Tang, W. S.; Chotard, J.-N.; Raybaud, P.; Janot, R. Hydrogenation Properties of KSi and $NaSi$ Zintl Phases. *Phys. Chem. Chem. Phys.* **2012**, *14* (38), 13319–13324.
- (3) Tang, W. S.; Chotard, J.-N.; Raybaud, P.; Janot, R. Enthalpy–Entropy Compensation Effect in Hydrogen Storage Materials: Striking Example of Alkali Silanides $MSiH_3$ ($M = K, Rb, Cs$). *J. Phys. Chem. C* **2014**, *118* (7), 3409–3419.
- (4) Jain, A.; Ichikawa, T.; Yamaguchi, S.; Miyaoka, H.; Kojima, Y. Catalytic Modification in Dehydrogenation Properties of $KSiH_3$. *Phys. Chem. Chem. Phys.* **2014**, *16* (47), 26163–26167.
- (5) Kranak, V. F.; Lin, Y.-C.; Karlsson, M.; Mink, J.; Norberg, S. T.; Häussermann, U. Structural and Vibrational Properties of Silyl (SiH_3^-) Anions in $KSiH_3$ and $RbSiH_3$: New Insight into Si–H Interactions. *Inorg. Chem.* **2015**, *54* (5), 2300–2309.
- (6) Ring, M. A.; Ritter, D. M. Preparation and Reactions of Potassium Silyl. *J. Am. Chem. Soc.* **1961**, *83* (4), 802–805.
- (7) Ring, M. A.; Ritter, D. M. Crystal Structure of Potassium Silyl. *J. Phys. Chem.* **1961**, *65* (1), 182–183.
- (8) Weiss, E.; Hencken, G.; Kühn, H. Kristallstrukturen Und Kernmagnetische Breitlinienresonanz Der Alkalisilyle SiH_3M ($M = K, Rb, Cs$). *Chem. Ber.* **1970**, *103* (9), 2868–2872.
- (9) Mundt, O.; Becker, G.; Hartmann, H.-M.; Schwarz, W. Metallderivate von Molekülverbindungen. II. Darstellung Und Struktur Des β -Kaliumsilanids. *Z. Anorg. Allg. Chem.* **1989**, *572* (1), 75–88.
- (10) Raybaud, P.; Ropital, F. [Institute Francais Du Petrol (IFP)]. Procédé pour le stockage de l'hydrogène mettant en jeu un système équilibré entre un alliage de métal alcalin et de silicium et l'hydrure correspondant. International Patent WO 2006/082315, Jun 10, 2006.
- (11) Amberger, E.; Römer, R.; Layer, A. Reaktionen Der Hydrylanionen V. Darstellung von SiH_3Na , SiH_3K , SiH_3Rb , SiH_3Cs Und SnH_3K Und Ihre Umsetzung Mit CH_3J . *J. Organomet. Chem.* **1968**, *12* (3), 417–423.
- (12) Fehér, F.; Krancher, M. Beiträge Zur Chemie Des Siliciums Und Germaniums. XXXIV. Ein Weiterer Beitrag Zur Darstellung von Kaliumsilyl. *Z. Anorg. Allg. Chem.* **1984**, *509* (2), 95–100.
- (13) Tang, W. S.; Chotard, J.-N.; Janot, R. Synthesis of Single-Phase $LiSi$ by Ball-Milling: Electrochemical Behavior and Hydrogenation Properties. *J. Electrochem. Soc.* **2013**, *160* (8), A1232–A1240.
- (14) Österberg, C.; Fahlquist, H.; Häussermann, U.; Brown, C. M.; Udovic, T. J.; Karlsson, M. Dynamics of Pyramidal SiH_3^- Ions in $ASiH_3$ ($A = K$ and Rb) Investigated with Quasielastic Neutron Scattering. *J. Phys. Chem. C* **2016**, *120* (12), 6369–6376.
- (15) Stockmayer, W. H.; Stephenson, C. C. The Nature of the Gradual Transition in Sodium Borohydride. *J. Chem. Phys.* **1953**, *21* (7), 1311–1312.
- (16) Abrahams, S. C.; Kalnajs, J. The Lattice Constants of the Alkali Borohydrides and the Low-Temperature Phase of Sodium Borohydride. *J. Chem. Phys.* **1954**, *22* (3), 434–436.
- (17) Soldate, A. M. Crystal Structure of Sodium Borohydride. *J. Am. Chem. Soc.* **1947**, *69* (5), 987–988.
- (18) Stephenson, C. C.; Rice, D. W.; Stockmayer, W. H. Order–Disorder Transitions in the Alkali Borohydrides. *J. Chem. Phys.* **1955**, *23* (10), 1960–1960.

- (19) Evers, J.; Oehlinger, G.; SEXTL, G. High-Pressure Synthesis of LiSi: Three-Dimensional Network of Three-Bonded Si⁻ Ions. *Angew. Chem., Int. Ed. Engl.* **1993**, *32* (10), 1442–1444.
- (20) Evers, J.; Oehlinger, G.; SEXTL, G. ChemInform Abstract: LiSi, a Unique Zintl Phase — Although Stable, It Long Evaded Synthesis. *ChemInform* **1998**, *29* (13), no–no.
- (21) Goebel, T.; Prots, Y.; Haarmann, F. Refinement of the Crystal Structure of Tetrasodium Tetrasilicide, Na₄Si₄. *Z. Kristallogr. - New Cryst. Struct.* **2008**, *223* (3), 187–188.
- (22) von Schnering, H. G.; Schwarz, M.; Chang, J.-H.; Peters, K.; Peters, E.-M.; Nesper, R. Refinement of the Crystal Structures of the Tetrahydrotetrasilicides K₄Si₄, Rb₄Si₄ and Cs₄Si₄. *Z. Kristallogr. - New Cryst. Struct.* **2005**, *220* (4), 525–527.
- (23) Waibel, M.; Raudaschl-Sieber, G.; Fässler, T. F. Mixed Tetrahedral Zintl Clusters: Single Crystal Structure Determination of [Si_{4-x}Ge_x]₄⁻, [(MesCu)₂(Si_{4-x}Ge_x)₄]⁻, and the ²⁹Si MAS NMR Spectra of A₄Si₂Ge₂ (A = K, Rb). *Chem. - Eur. J.* **2011**, *17* (48), 13391–13394.
- (24) The mention of all commercial suppliers in this article is for clarity. This does not imply the recommendation or endorsement of these suppliers by NIST.
- (25) Rodríguez-Carvajal, J. Recent Advances in Magnetic Structure Determination by Neutron Powder Diffraction. *Phys. B* **1993**, *192* (1), 55–69.
- (26) Boulton, A.; Louër, D. Powder Pattern Indexing with the Dichotomy Method. *J. Appl. Crystallogr.* **2004**, *37* (5), 724–731.
- (27) Laugier, J.; Bochu, B. *LMGP-Suite: Suite of Programs for the Interpretation of X-ray Experiments*; ENSP/Laboratoire des Matériaux et du Génie Physique: Saint Martin d'Hères, France, 2003.
- (28) Favre-Nicolin, V.; Černý, R. FOX, 'free Objects for Crystallography': a Modular Approach to *Ab Initio* Structure Determination from Powder Diffraction. *J. Appl. Crystallogr.* **2002**, *35* (6), 734–743.
- (29) Gelato, L. M.; Parthé, E. *STRUCTURE TIDY* – a Computer Program to Standardize Crystal Structure Data. *J. Appl. Crystallogr.* **1987**, *20* (2), 139–143.
- (30) Momma, K.; Izumi, F. VESTA 3 for Three-Dimensional Visualization of Crystal, Volumetric and Morphology Data. *J. Appl. Crystallogr.* **2011**, *44* (6), 1272–1276.
- (31) Udovic, T. J.; Brown, C. M.; Leão, J. B.; Brand, P. C.; Jiggetts, R. D.; Zeitoun, R.; Pierce, T. A.; Peral, I.; Copley, J. R. D.; Huang, Q.; et al. The Design of a Bismuth-Based Auxiliary Filter for the Removal of Spurious Background Scattering Associated with Filter-Analyzer Neutron Spectrometers. *Nucl. Instrum. Methods Phys. Res., Sect. A* **2008**, *588* (3), 406–413.
- (32) Meyer, A.; Dimeo, R. M.; Gehring, P. M.; Neumann, D. A. The High-Flux Backscattering Spectrometer at the NIST Center for Neutron Research. *Rev. Sci. Instrum.* **2003**, *74* (5), 2759–2777.
- (33) Copley, J. R. D.; Cook, J. C. The Disk Chopper Spectrometer at NIST: A New Instrument for Quasielastic Neutron Scattering Studies. *Chem. Phys.* **2003**, *292* (2–3), 477–485.
- (34) Azuah, R. T.; Kneller, L. R.; Qiu, Y.; Tregenna-Piggott, P. L. W.; Brown, C. M.; Copley, J. R. D.; Dimeo, R. M. DAVE: A Comprehensive Software Suite for the Reduction, Visualization, and Analysis of Low Energy Neutron Spectroscopic Data. *J. Res. Natl. Inst. Stand. Technol.* **2009**, *114*, 341–358.
- (35) Giannozzi, P.; Baroni, S.; Bonini, N.; Calandra, M.; Car, R.; Cavazzoni, C.; Ceresoli, D.; Chiarotti, G. L.; Cococcioni, M.; Dabo, I.; et al. QUANTUM ESPRESSO: A Modular and Open-Source Software Project for Quantum Simulations of Materials. *J. Phys.: Condens. Matter* **2009**, *21* (39), 395502.
- (36) Kresse, G.; Furthmüller, J.; Hafner, J. *Ab Initio* Force Constant Approach to Phonon Dispersion Relations of Diamond and Graphite. *EPL Europhys. Lett.* **1995**, *32* (9), 729.
- (37) Yildirim, T. Structure and Dynamics from Combined Neutron Scattering and First-Principles Studies. *Chem. Phys.* **2000**, *261* (1–2), 205–216.
- (38) Udovic, T. J.; Verdal, N.; Rush, J. J.; De Vries, D. J.; Hartman, M. R.; Vajo, J. J.; Gross, A. F.; Skripov, A. V. Mapping Trends in the Reorientational Mobilities of Tetrahydroborate Anions via Neutron-Scattering Fixed-Window Scans. *J. Alloys Compd.* **2013**, *580* (Suppl. 1), S47–S50.
- (39) Bée, M. *Quasielastic Neutron Scattering: Principles and Applications in Solid State Chemistry, Biology and Materials Science*; Adam Hilger: Bristol, U.K., 1988.
- (40) Verdal, N.; Udovic, T. J.; Rush, J. J.; Liu, X.; Majzoub, E. H.; Vajo, J. J.; Gross, A. F. Dynamical Perturbations of Tetrahydroborate Anions in LiBH₄ due to Nanoconfinement in Controlled-Pore Carbon Scaffolds. *J. Phys. Chem. C* **2013**, *117* (35), 17983–17995.
- (41) Verdal, N.; Udovic, T. J.; Stavila, V.; Tang, W. S.; Rush, J. J.; Skripov, A. V. Anion Reorientations in the Superionic Conducting Phase of Na₂B₁₂H₁₂. *J. Phys. Chem. C* **2014**, *118* (31), 17483–17489.
- (42) Udovic, T. J.; Matsuo, M.; Tang, W. S.; Wu, H.; Stavila, V.; Solonin, A. V.; Skoryunov, R. V.; Babanova, O. A.; Skripov, A. V.; Rush, J. J.; et al. Exceptional Superionic Conductivity in Disordered Sodium Decahydro-closo-decaborate. *Adv. Mater.* **2014**, *26* (45), 7622–7626.